

MelT: GEMM-Native NDFT for Efficient Single-Stage Audio Frontends on Modern Accelerators

Augusto Camargo¹ and Marcelo Finger¹

¹Instituto de Ciências Matemáticas e de Computação, University of São Paulo, Brazil
 augustoc@usp.br, mfinger@ime.usp.br

June 2, 2026

Abstract

Modern audio processing networks are commonly deployed on accelerators whose peak throughput is obtained through dense linear algebra, whereas conventional acoustic frontends—a Short-Time Fourier Transform (STFT) followed by sparse Mel aggregation—remain structurally heterogeneous. This mismatch can introduce memory-bandwidth, dispatch, and intermediate-allocation overheads on contemporary accelerator backends. This work introduces MelT, a single-stage frontend framework in which Mel-spaced Non-Uniform Discrete Fourier Transform (NDFT) bases are precomputed and applied to time-domain acoustic frames through dense General Matrix Multiplication (GEMM) operations. The contribution is not the NDFT operator itself; rather, it is the formulation of Mel-spaced NDFT projection as a GEMM-native audio frontend and its evaluation as a hardware-efficient alternative to conventional STFT+Mel pipelines. Evaluated across platforms ranging from Apple A18 Pro edge hardware to NVIDIA H100 datacenter acceleration, MelT attains up to a $3.75\times$ speedup in inference latency and a $3.52\times$ reduction in energy consumption while maintaining downstream classification accuracy.

1 Introduction

Large-scale audio systems—including speech recognizers [1], audio classifiers [2,3], and self-supervised models [4]—are increasingly deployed on hardware optimized for dense matrix multiplication. Nevertheless, the dominant frontend architecture used by these systems remains a multi-stage pipeline consisting of a Short-Time Fourier Transform (STFT) followed by sparse Mel filterbank aggregation. This classical pipeline was designed around the algorithmic efficiency of the Cooley–Tukey FFT [5], rather than the dense matrix engines, Tensor Cores [6], or specialized matrix coprocessors [7] that dominate modern inference throughput. As a result, each frontend evaluation can incur additional memory traffic, kernel dispatch overhead, intermediate tensor allocation, and underutilization of matrix-oriented silicon.

To address this hardware mismatch, this work introduces **MelT**, a single-stage frontend framework that reformulates acoustic feature extraction by replacing the decoupled STFT and sparse filterbank stages with a GEMM-native dense projection at Mel-spaced frequencies. By leveraging the established mathematical foundation of the Non-Uniform Discrete Fourier Transform (NDFT) [8], MelT evaluates arbitrary Mel-spaced frequency coordinates directly in the target representation. Unlike prior uses of NDFT as a general spectral operator, the focus here is its role as a direct Mel-space frontend whose computation can be expressed as dense matrix multiplication and evaluated

across heterogeneous accelerator platforms. Its cepstral extension, **MFCCT**, is evaluated as a hardware-native analogue of conventional Mel-Frequency Cepstral Coefficients (MFCC). Benchmarked across four hardware accelerator generations (NVIDIA H100, NVIDIA V100, Apple M4 Pro, and Apple A18 Pro), MelT achieves a **1.92×–3.75× latency speedup** and up to a **3.52× reduction in energy consumption** relative to the conventional STFT+Mel pipeline. In addition, MFCCT achieves competitive downstream performance on a clinical respiratory classification task, obtaining a measured F_1 score of 0.9860, compared with 0.9737 for the baseline MFCC formulation. The primary contributions of this work are summarized as follows:

- A hardware-native formulation of Mel-spaced NDFT projection as a direct audio frontend, mapping time-domain waveforms into Mel-frequency coordinates through unified General Matrix Multiplication (GEMM) operations, together with an analysis showing that coherent direct projection and conventional incoherent post-energy Mel aggregation are not strictly algebraically equivalent (Section 3.1).
- A cross-platform latency and hardware-telemetry energy benchmark evaluating matmul-native audio frontends across four hardware acceleration generations spanning edge, workstation, and datacenter platforms (Section 4).
- Downstream task validation on VoxCeleb1 gender classification and SPIRA COVID-19 detection, indicating representation fidelity and competitive empirical performance for MFCCT relative to conventional baselines (Section 4).

2 Related Work

Audio frontends. The dominant audio frontend—short-time Fourier transform followed by triangular Mel filterbank aggregation—was introduced by Davis and Mermelstein [9] and has remained architecturally stable for four decades, despite relying on the Cooley–Tukey FFT [5], which was not designed around modern matrix-accelerator execution paths. Learnable frontends replace this fixed pipeline with trainable parameters: SincNet [10] learns sinc-based filters from raw waveform; LEAF [11] extends this approach with Gabor filters and per-channel energy normalization, at roughly 300× the compute cost of a fixed Mel spectrogram. EfficientLEAF [12] reduces that overhead to 3% of LEAF’s cost via inhomogeneous convolutions, yet concludes that *“both [LEAF and EfficientLEAF] fail to consistently outperform a fixed mel filterbank—the quest for learnable audio frontends is not solved”*. Neither learnable approach reports hardware energy measurements or cross-platform GPU benchmarks.

TMFWC [13] proposes a time-domain Mel-frequency representation by synthesizing Mel-spaced sinusoidal basis functions and computing feature magnitudes directly from time-domain projections. While conceptually related to MelT in avoiding the conventional STFT+Mel pipeline, the method is presented using wavelet terminology and does not explicitly formulate the operation within the NDFT framework. Moreover, TMFWC does not investigate accelerator-oriented implementations, dense GEMM execution, cross-platform benchmarking, or hardware energy consumption. MelT instead formulates Mel-spaced projection as a GEMM-native NDFT frontend and evaluates its latency, energy efficiency, and downstream behavior across heterogeneous accelerator platforms. A structural comparison between TMFWC and MelT is summarized in Table 1.

Dense matrix formulations in signal processing. The Non-Uniform Discrete Fourier Transform (NDFT) has been studied in signal processing [14] and geophysical processing [15]. Unlike the FFT, which evaluates the spectrum on a uniform frequency grid, the NDFT evaluates the Fourier transform at arbitrary frequency nodes and can be implemented as a matrix multiplication against

Table 1: Architectural and structural comparison between TMFWC and MelT.

Property / Feature	TMFWC [13]	MelT
Time-Domain Mel Representation	Yes	Yes
Time-Domain Mel Basis Functions	Yes	Yes
Magnitude from Real/Imaginary Components	Yes	Yes
Explicit NDFT Formulation	No	Yes
Dense GEMM Formulation	No	Yes
Accelerator-Oriented Design	No	Yes
Cross-Platform Benchmarking	No	Yes
Chip-Level Energy Telemetry	No	Yes

a precomputed basis matrix. Lin [16] formulated the NDFT as a GPU-resident tensor operation for non-Cartesian MRI reconstruction, reporting 5–13× acceleration over CPU implementations. Potts et al. [8] provide a widely cited tutorial on fast algorithms for nonequispaced Fourier transforms. These works establish that NDFT-as-matmul is computationally viable on modern accelerators. A review of the current literature indicates that prior work has not evaluated GEMM-native NDFT projection as a direct Mel-space audio frontend across heterogeneous accelerator platforms.

Energy measurement in AI inference. Schwartz et al. [17] argue that computational efficiency—including energy—should be a first-class evaluation criterion in AI research alongside accuracy, coining the term *Green AI*. Caspart et al. [18] demonstrate precise GPU energy measurement via NVML for heterogeneous deep learning workloads, establishing that runtime alone is insufficient to estimate energy consumption: actual power draw must be sampled directly from hardware counters. This methodology is adopted here—NVML on NVIDIA platforms and `powermetrics` on Apple SoCs—and applied to audio frontend inference, a setting for which chip-level frontend telemetry is rarely reported.

3 Methodology

3.1 Matmul-Native Mel Frontends

Conventional Mel frontends follow a multi-stage approach in which a linear-frequency spectrum is computed before sparse integration into the Mel scale. In contrast, Direct Mel Projection operates directly at the target Mel-spaced frequency coordinates, thereby avoiding intermediate linear-frequency spectral tensors.

Let $x[n]$ denote a discrete-time signal sampled at frequency f_s . Following framing and windowing procedures, Mel-spaced projection frequencies are defined through the Mel scale:

$$\mu(f) = 2595 \log_{10} \left(1 + \frac{f}{700} \right). \tag{1}$$

For M projection frequencies bounded between f_{\min} and f_{\max} , the target Mel locations are uniformly distributed as:

$$\mu_m = \mu_{\min} + \frac{m+1}{M+1} (\mu_{\max} - \mu_{\min}), \quad m = 0, \dots, M-1, \tag{2}$$

where the physical boundaries are defined by:

$$\mu_{\min} = 2595 \log_{10} \left(1 + \frac{f_{\min}}{700} \right), \quad \mu_{\max} = 2595 \log_{10} \left(1 + \frac{f_{\max}}{700} \right). \tag{3}$$

The corresponding analysis frequencies in hertz are obtained via the inverse Mel mapping:

$$f_m = 700 \left(10^{\mu_m/2595} - 1 \right). \quad (4)$$

Let $x_t[n]$ denote the t -th framed signal segment and $\tilde{x}_t[n] = w[n]x_t[n]$ its windowed version. For a windowed discrete signal frame $\tilde{x}_t[n]$, Direct Mel Projection computes the real and imaginary components through:

$$R_{t,m} = \sum_{n=0}^{N-1} \tilde{x}_t[n] \cos \left(\frac{2\pi f_m n}{f_s} \right), \quad (5)$$

$$I_{t,m} = \sum_{n=0}^{N-1} \tilde{x}_t[n] \sin \left(\frac{2\pi f_m n}{f_s} \right). \quad (6)$$

The resulting Mel-spaced projection energy is defined as:

$$S_{t,m} = R_{t,m}^2 + I_{t,m}^2. \quad (7)$$

Unlike conventional Mel filtering, in which power values are first computed on uniformly spaced FFT bins and then aggregated through nonnegative triangular weights, Eq. (7) applies a coherent time-domain projection before magnitude-squared energy resolution. Consequently, Direct Mel Projection should be interpreted as a Mel-spaced NDFT frontend rather than as an algebraically exact rearrangement of the conventional STFT+Mel computation.

Equivalently, the sequence can be expressed natively as dense matrix multiplications. Let $\mathbf{X} \in \mathbb{R}^{T \times N}$ denote the matrix composed of stacked unwindowed acoustic frames, such that windowing is absorbed into the fixed projection matrices. Fixed projection matrices are precomputed:

$$\mathbf{W}_{m,n}^{(r)} = w[n] \cos \left(\frac{2\pi f_m n}{f_s} \right), \quad \mathbf{W}_{m,n}^{(i)} = w[n] \sin \left(\frac{2\pi f_m n}{f_s} \right). \quad (8)$$

The parallelized matrix projection pass is then formulated as:

$$\mathbf{R} = \mathbf{X} \left(\mathbf{W}^{(r)} \right)^\top, \quad \mathbf{I} = \mathbf{X} \left(\mathbf{W}^{(i)} \right)^\top, \quad (9)$$

with Mel-scale projection energies resolved via element-wise Hadamard multiplication (\odot):

$$\mathbf{S} = \mathbf{R} \odot \mathbf{R} + \mathbf{I} \odot \mathbf{I}. \quad (10)$$

Subsequent frontend variants differ only in the operations applied to the resulting matrix \mathbf{S} .

3.1.1 MelT Formulation

MelT (Mel Transform Frontend) applies logarithmic compression directly to the extracted matrix \mathbf{S} :

$$\mathbf{M}^{\text{MelT}} = \log(\mathbf{S} + \epsilon) = \log \left((\mathbf{X}(\mathbf{W}^{(r)})^\top) \odot (\mathbf{X}(\mathbf{W}^{(r)})^\top) + (\mathbf{X}(\mathbf{W}^{(i)})^\top) \odot (\mathbf{X}(\mathbf{W}^{(i)})^\top) + \epsilon \right). \quad (11)$$

3.1.2 MFCCT Formulation

MFCCT is defined as the cepstral extension of the Direct Mel Projection paradigm by applying an orthonormal Discrete Cosine Transform (DCT-II) matrix $\mathbf{D} \in \mathbb{R}^{K \times M}$ to the log-compressed representation:

$$\mathbf{C}^{\text{MFCCT}} = \mathbf{M}^{\text{MelT}} \mathbf{D}^\top = \log(\mathbf{S} + \epsilon) \mathbf{D}^\top. \quad (12)$$

The computational distinction between conventional MFCC and the proposed MFCCT frontend is illustrated in Fig. 1.

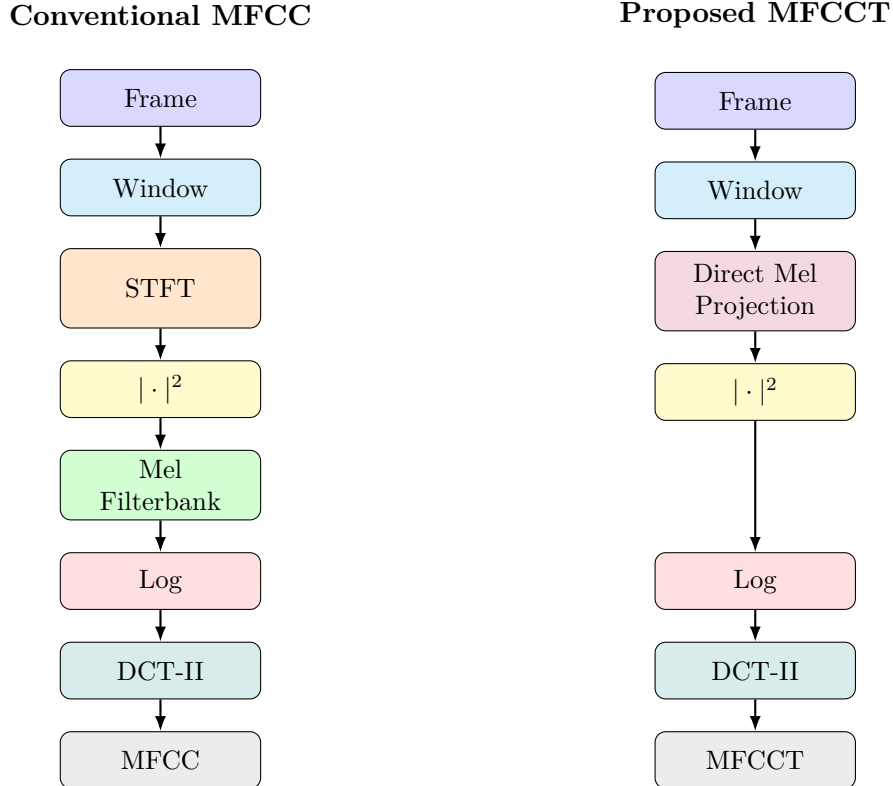


Figure 1: Computational layout comparing conventional MFCC extraction with the proposed matmul-dense MFCCT frontend configuration.

3.2 Computational Complexity and Architectural Realization

A standard sequential audio frontend evaluates windowed data through an intermediate linear-frequency spectrum before aggregation. Let N denote the window frame length, M the number of target Mel frequency bins, and T the total number of frames. For a single frame, a standard radix-2 FFT requires $\mathcal{O}(N \log_2 N)$ operations, followed by sparse Mel filterbank multiplication:

$$\text{Complexity}_{\text{Conventional}} = \mathcal{O}(N \log_2 N + \text{nnz}(\mathbf{F}_{\text{Mel}})), \quad \text{nnz}(\mathbf{F}_{\text{Mel}}) \leq M \left(\frac{N}{2} + 1 \right). \quad (13)$$

In contrast, evaluating the Mel-spaced NDFT basis directly at the target frequencies yields the following per-frame arithmetic scaling:

$$\text{Complexity}_{\text{Proposed}} = \mathcal{O}(N \cdot M). \quad (14)$$

For a full utterance, both expressions scale linearly with T before accelerator-level parallelization.

Asymptotically, FFT-based approaches remain mathematically favorable when N is large and hardware effects are abstracted away. However, latency on modern deep learning accelerators is often not determined by floating-point operation count alone; kernel launch overhead, intermediate tensor allocation, memory traffic, sparse indexing, and cache behavior can dominate realized runtime. Mapping feature extraction into dense General Matrix Multiplication (GEMM) operations exposes a regular compute pattern with high arithmetic intensity and mature accelerator support. The resulting formulation trades asymptotic FFT efficiency for a hardware-native execution path that is better aligned with tensor-oriented accelerator backends in the compact- M regime typical of neural audio frontends.

Table 2: Hardware platforms used for evaluation.

Tier	Platform	Memory	Backend
Edge	Apple A18 Pro	Unified	MLX / MPS
Workstation	Apple M4 Pro	Unified	MLX / MPS
Legacy Datacenter	Tesla V100	32 GB	CUDA + TF32
Modern Datacenter	H100	80 GB HBM3	CUDA + TF32

Table 3: Audio frontend configuration.

Parameter	Spectral	Cepstral
Sample Rate	16 kHz	16 kHz
Frame Length N	400 (25 ms)	1200 (75 ms)
Hop Size H	160 (10 ms)	160 (10 ms)
Mel Bins M	80	128
MFCC Coefficients K	–	13
f_{\min}	80 Hz	0 Hz
f_{\max}	7600 Hz	8000 Hz

4 Experiments and Results

4.1 Experimental Setup

Hardware Infrastructure. Evaluation was conducted across four execution platforms spanning edge, workstation, and datacenter deployment settings, as summarized in Table 2. NVIDIA results were obtained with PyTorch CUDA and TF32 enabled. Apple results used the fastest available backend per (frontend, duration) pair among PyTorch MPS and MLX GPU.

Audio Configuration. All benchmarks used real LibriSpeech speech signals resampled to 16 kHz, with durations ranging from 1 s to 160 s. Frontend parameters are summarized in Table 3. Cepstral configurations were selected to maintain structural symmetry with standard `librosa` implementations [19].

Statistical Methodology. Each (frontend, backend, duration) configuration was measured across 20 independent trials. Each individual trial computed the median of 200 timed execution calls following 50 explicit warmup iterations. Reported metrics reflect the median of the 20 distinct trial medians, providing robustness against transient system interrupt noise.

Energy Measurement. NVIDIA platforms employed NVML telemetry via `nvmlDeviceGetPowerUsage`, sampled at a 100 ms frequency during repeated-call measurement windows. Apple platforms used the `powermetrics` profiling tool to capture full chip-level power draw, including CPU and GPU activity. Total inference energy was computed as $E = \bar{P} \times \bar{t}$, where \bar{P} denotes the median sampled power during the measurement window and \bar{t} denotes the median per-call latency. Because hardware power counters have coarser temporal resolution than individual sub-millisecond frontend calls, power is interpreted as steady-state draw over repeated execution windows rather than as instantaneous per-call telemetry. Accordingly, energy values are interpreted as within-platform comparisons between frontend implementations rather than as absolute cross-platform energy rankings.

Table 4: Performance and energy comparison between the conventional STFT+Mel pipeline and the proposed MelT frontend at the maximum evaluated context length (160s). Metrics correspond to the fastest available backend for each frontend across PyTorch CUDA, MPS, CPU, and MLX runtimes.

Platform	Latency (ms) STFT+Mel / MelT	Speedup	Energy (mJ) STFT+Mel / MelT	Energy Reduction	STFT Power (W) Median [P25, P75]	MelT Power (W) Median [P25, P75]
H100 80GB	0.145/0.076	1.92 \times	63.4/23.2	2.74 \times	438.1 [438.0, 438.2]	309.0 [308.5, 309.1]
V100 32GB	0.468/0.345	1.36 \times	109.5/90.9	1.20 \times	233.9 [233.8, 234.1]	263.4 [262.7, 264.2]
M4 Pro	1.362/0.914	1.49 \times	45.8/13.5	3.40 \times	17.3 [17.3, 17.4]	16.0 [15.8, 17.1]
A18 Pro	9.981/2.664	3.75 \times	37.3/10.6	3.52 \times	3.68 [3.66, 3.69]	3.71 [3.71, 3.72]

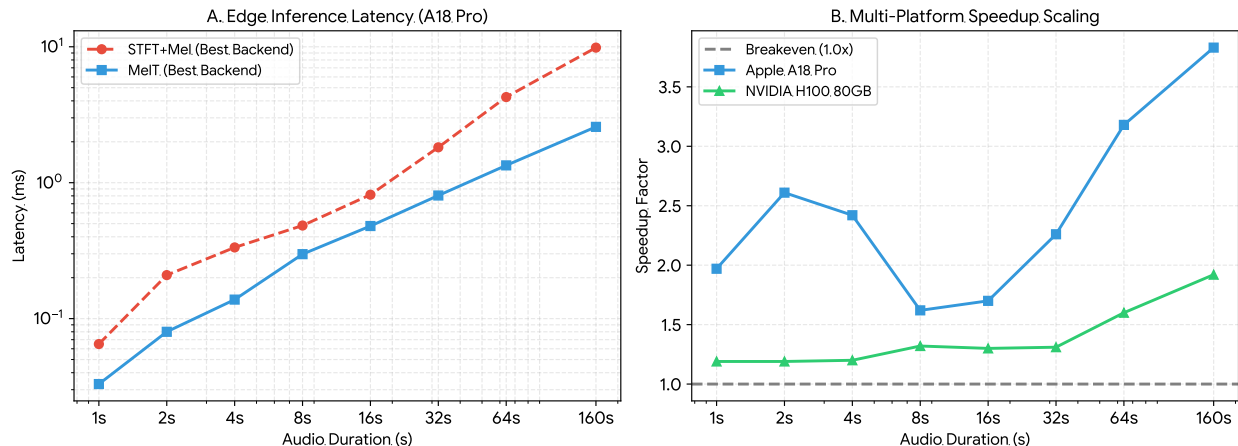


Figure 2: Latency scaling (Panel A) and corresponding speedup (Panel B) of MelT relative to the conventional STFT+Mel pipeline. Panel A shows edge inference latency on the Apple A18 Pro, while Panel B shows speedup scaling on the Apple A18 Pro and NVIDIA H100 for input durations ranging from 1 s to 160 s.

4.2 Latency and Throughput Analysis

Table 4 summarizes latency performance at the maximum evaluated signal duration of 160 s. Acceleration gains increase with input duration across the evaluated architectures, as shown empirically in the two panels of Fig. 2. At the shortest evaluated duration (1 s), backend dispatch overheads remain visible, yielding a modest 1.19 \times speedup on the H100 and an approximately 2 \times speedup on the A18 Pro, as shown in Fig. 2, Panel B. As audio duration increases to 160 s, the matmul-dense formulation enters a higher-throughput execution regime, establishing latency reductions of 1.92 \times and 3.75 \times , respectively. On the Apple M4 Pro workstation, a 160 s signal requires 1.362 ms with the conventional pipeline, whereas the same segment is processed by MelT in 0.914 ms, consistent with reduced irregular indexing and improved utilization of matrix-oriented execution paths.

4.3 Energy Footprint and Sustainability Metrics

As shown in Table 4 and visualized in Fig. 3, energy reductions can exceed latency gains when lower execution time is accompanied by reduced chip-level power draw. On the H100, processing the maximum context yields a median hardware draw of 438.1 W under the conventional STFT+Mel

pipeline, whereas the dense Direct Mel Projection path yields 309.0 W. This corresponds to a 29.4% reduction in median power draw, which combines with the latency improvement to produce a $2.74\times$ reduction in active energy. On the A18 Pro, median power remains approximately constant between the two frontends (3.68 W vs. 3.71 W); therefore, the $3.52\times$ energy reduction is primarily attributable to shorter active execution time rather than lower instantaneous power.

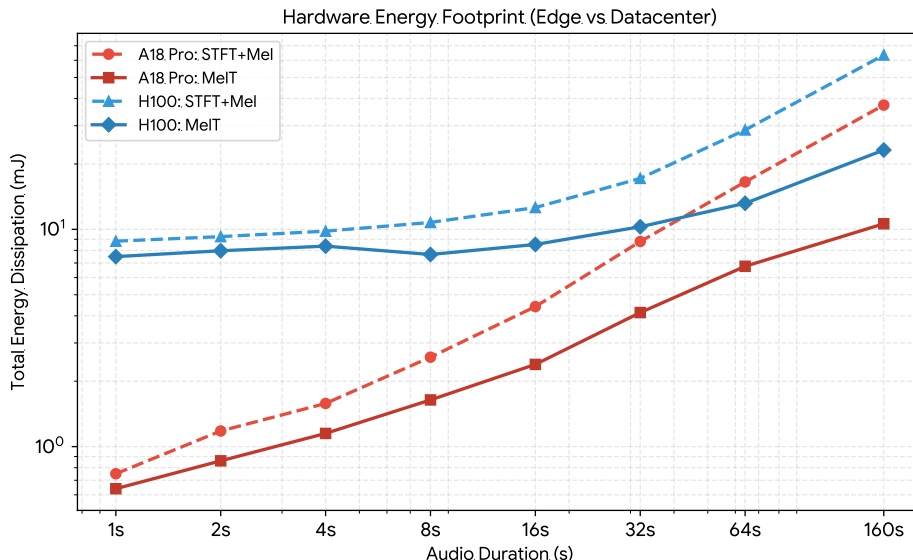


Figure 3: Hardware energy consumption in millijoules over a logarithmic execution scaling continuum.

4.4 Representation Fidelity and Downstream Invariance

To quantify the downstream impact of coherent versus incoherent frequency aggregation, frame-level feature matrices were compared using cosine similarity metrics. The structural similarity between MelT and STFT+Mel consistently remains between 0.93 and 0.95, indicating close spatial alignment despite the different order of projection and energy aggregation operations.

Table 5: Respiratory deficit classification metrics on the SPIRA dataset.

	Baseline MFCC (Test)	MFCCT (CV Mean \pm Std)	MFCCT (Test)
Accuracy	0.9719	0.9686 \pm 0.0134	0.9851
Precision	0.9663	0.9644 \pm 0.0121	0.9845
Recall	0.9813	0.9903 \pm 0.0098	0.9875
F_1 Score	0.9737	0.9772 \pm 0.0099	0.9860
AUC	0.9976	0.9909 \pm 0.0108	0.9993

Downstream evaluation on VoxCeleb1 [20] gender classification (Table 6) indicates comparable feature utility, with MFCCT remaining within 0.2 percentage points of the standard MFCC baseline (97.84% vs. 97.95%). Cross-evaluation metrics further indicate that models trained on conventional STFT-derived feature vectors retain substantial performance when evaluated on matmul-native features. On clinical respiratory tasks using SPIRA COVID-19 classifiers (Table 5), MFCCT yields higher measured test metrics, increasing F_1 score from 0.9737 to 0.9860. This observed improvement may be related to coherent projection prior to energy resolution, although further

Table 6: Gender classification accuracy on VoxCeleb1. Cross-evaluation tests representations trained with the conventional baseline frontend and evaluated with the matmul-native frontend.

Frontend Target	Same-Frontend Acc.	Cross-Eval Acc.
Standard MFCC	97.95%	N/A
MFCCT	97.84%	96.51%
Traditional STFT+Mel	88.81%	N/A
MelT	88.91%	85.52%

Table 7: Maximum observed acceleration and energy reduction of MFCCT relative to conventional MFCC extraction at 160s.

Platform	Latency Gain	Energy Gain
Apple A18 Pro	3.65×	3.39×
Apple M4 Pro	1.51×	3.15×
NVIDIA H100	1.85×	2.51×
NVIDIA V100	1.35×	1.20×

empirical investigation and statistical validation are required to characterize the underlying structural effects. The present work does not attempt to establish statistical superiority of MFCCT over MFCC; the reported results should be interpreted as empirical observations motivating future investigation.

4.5 Computational Generalization to MFCCT

Because MFCCT reuses the same GEMM-native Direct Mel Projection stage employed by MelT and differs only through the addition of logarithmic compression and a fixed DCT-II transform, similar computational behavior is expected. To verify that the observed hardware benefits are not specific to the MelT representation, MFCC and MFCCT were benchmarked on the same hardware platforms and evaluation protocol.

As shown in Table 7, the cepstral extension preserves the computational advantages of the proposed formulation across all evaluated hardware platforms. The largest gains are observed on Apple Silicon devices, where MFCCT achieves up to a 3.65× latency reduction and a 3.39× reduction in energy consumption relative to conventional MFCC extraction. Similar trends are observed on datacenter accelerators, indicating that the benefits of matmul-native frontend computation extend beyond MelT and remain present after cepstral transformation.

4.6 Scaling with the Number of Mel Bins

To empirically characterize the scaling behavior implied by the $\mathcal{O}(NM)$ projection cost, an additional sweep was performed over the number of Mel bins M on the NVIDIA H100 at the maximum evaluated context length of 160s.

As shown in Table 8, the speedup decreases monotonically as M increases, consistent with the expected $\mathcal{O}(NM)$ arithmetic scaling of Direct Mel Projection. Nevertheless, the proposed formulation remains advantageous throughout the 40–512 Mel-bin range evaluated in this study. In particular, MelT retains speedups of 1.88× and 1.75× at $M = 80$ and $M = 128$, respectively, corresponding to the operating regime commonly used by contemporary neural audio frontends. The results therefore indicate that the practical crossover point occurs near the upper end of the

Table 8: MelT speedup relative to the conventional STFT+Mel pipeline as a function of the number of Mel bins M on the NVIDIA H100 at 160s.

Mel Bins (M)	Speedup
40	2.08×
80	1.92×
128	1.75×
256	1.39×
512	1.01×

evaluated range, while MelT remains advantageous in the Mel-resolution regime typically employed in modern speech and audio systems.

4.7 Code and Artifact Availability

The source code, benchmark scripts, configuration files, and aggregated experimental results used in this work are publicly available at:

https://github.com/augustocamargo/MelT_arxiv

5 Discussion

The central contribution of this work is therefore not a new spectral transform, but the observation that Mel-space projection can be reformulated as a GEMM-native computation whose hardware behavior differs substantially from conventional STFT-based frontends. Conventional audio pipelines were historically designed around the asymptotic efficiency of FFT-based algorithms, whereas modern inference hardware increasingly derives performance from dense matrix multiplication engines. Consequently, theoretical operation count alone is often insufficient to predict realized latency.

Across all evaluated platforms, MelT consistently reduced execution time relative to the conventional STFT+Mel pipeline. The magnitude of the improvement varied by architecture, ranging from 1.36× on the NVIDIA V100 to 3.75× on the Apple A18 Pro. This variability suggests that frontend performance is influenced not only by arithmetic complexity, but also by backend-specific factors such as kernel dispatch overhead, intermediate tensor allocation, memory movement, and the efficiency of matrix-oriented execution paths. The larger gains observed on Apple Silicon indicate that unified-memory accelerators may benefit particularly strongly from reducing multi-stage frontend processing into a small number of dense operations.

The energy measurements further support this interpretation. On some platforms, such as the H100, energy reductions exceeded what would be expected from latency improvements alone because lower runtime coincided with reduced chip-level power draw. On others, such as the A18 Pro, power consumption remained approximately constant and energy savings were primarily attributable to shorter execution time. Together, these observations suggest that frontend restructuring can influence both execution efficiency and power behavior, depending on the underlying hardware architecture.

An important observation is that the computational advantages are not limited to MelT itself. The cepstral extension MFCCT reuses the same Direct Mel Projection stage and differs only through logarithmic compression and a fixed DCT-II transform. Despite this additional processing, MFCCT preserved the same qualitative latency and energy trends across all evaluated platforms. This result

suggests that the observed gains arise from the matmul-native projection mechanism rather than from a particular output representation, indicating that the approach may generalize to broader classes of spectral and cepstral frontends.

From a signal-processing perspective, Direct Mel Projection should not be interpreted as an algebraically exact reformulation of conventional Mel filtering. The two pipelines differ in the ordering of projection and energy aggregation operations, resulting in a coherent Mel-spaced projection rather than an incoherent aggregation of FFT-bin energies. Nevertheless, the downstream experiments indicate that these differences do not substantially degrade feature utility. Cosine similarities remained high, cross-evaluation experiments retained most classification performance, and MFCCT achieved competitive results, with improved measured performance on the SPIRA task. While these findings do not establish superiority of the representation itself, they suggest that substantial computational gains can be obtained without sacrificing practical effectiveness.

The principal limitation of the proposed formulation concerns scaling. As shown in Table 8, the measured speedup decreases as M increases, consistent with the expected $\mathcal{O}(NM)$ arithmetic growth. FFT-based methods retain a favorable asymptotic complexity of $\mathcal{O}(N \log_2 N)$, whereas Direct Mel Projection scales as $\mathcal{O}(NM)$. Consequently, the proposed approach is most attractive in the compact-bin regime commonly used by modern neural audio systems, where M typically lies between 64 and 128. The present study focuses on this practical operating region. Future work should further characterize this crossover across additional frame lengths, frontend parameterizations, accelerator architectures, and larger downstream tasks.

Overall, the results support a broader systems-level observation: as AI accelerators continue to evolve toward increasingly specialized dense linear algebra hardware, signal-processing frontends designed around matrix-native execution may become preferable to architectures optimized primarily for classical algorithmic complexity. In this context, MelT and MFCCT represent examples of a more general design philosophy in which frontend computation is co-designed with the execution characteristics of modern inference hardware.

6 Conclusion

This work demonstrates that conventional multi-stage acoustic frontends can be redesigned to align with the dense matrix multiplication paradigms that dominate modern deep learning hardware. By formulating Direct Mel Projection as a unified dense NDFT-based projection, intermediate linear-frequency spectral allocations are avoided and the frontend is expressed through accelerator-friendly GEMM operations. This architectural change achieves up to a $3.75\times$ speedup in inference latency and a corresponding $3.52\times$ reduction in hardware energy footprint while maintaining downstream classification accuracy across both speech identification and clinical diagnostic classification tasks. Similar computational trends were observed for the cepstral extension MFCCT, indicating that the benefits of the proposed formulation extend beyond a single frontend representation.

The NDFT-as-matmul identity itself is not claimed as a novel mathematical result. The contribution instead lies in formulating Mel-spaced NDFT projection as a GEMM-native audio frontend and evaluating its latency, energy, representation fidelity, and downstream behavior across heterogeneous accelerator platforms. The results further indicate that these computational advantages persist after cepstral transformation, suggesting that matmul-native frontend design may generalize to broader classes of audio representations.

As specialized deep learning accelerators continue to prioritize dense matrix operations over irregular sequential logic paths, signal-processing frontends designed around matrix-native execution may become increasingly attractive. In this context, MelT and MFCCT illustrate how classical audio

feature extraction can be reformulated to better exploit contemporary hardware while preserving practical utility for downstream machine learning tasks.

References

- [1] A. Radford, J. W. Kim, C. Hallacy, A. Ramesh, G. Goh, S. Agarwal, G. Sastry, A. Askell, P. Mishkin, J. Clark, G. Krueger, and I. Sutskever, “Robust speech recognition via large-scale weak supervision,” *arXiv preprint arXiv:2212.04356*, 2022.
- [2] S. Hershey, S. Chaudhuri, D. P. W. Ellis *et al.*, “CNN architectures for large-scale audio classification,” in *IEEE International Conference on Acoustics, Speech and Signal Processing (ICASSP)*, 2017, pp. 131–135.
- [3] Q. Kong, Y. Cao, T. Iqbal, Y. Wang, W. Wang, and M. D. Plumbley, “PANNs: Large-scale pretrained audio neural networks for audio pattern recognition,” *IEEE/ACM Transactions on Audio, Speech, and Language Processing*, vol. 28, pp. 2880–2894, 2020.
- [4] A. Baevski, H. Zhou, A. Mohamed, and M. Auli, “wav2vec 2.0: A framework for self-supervised learning of speech representations,” in *Advances in Neural Information Processing Systems (NeurIPS)*, vol. 33, 2020, pp. 12 449–12 460.
- [5] J. W. Cooley and J. W. Tukey, “An algorithm for the machine calculation of complex Fourier series,” *Mathematics of Computation*, vol. 19, no. 90, pp. 297–301, 1965.
- [6] S. Markidis, J. A. Der Chien, E. Laure, A. Podobas, and J. S. Vetter, “NVIDIA tensor core programmability, performance and precision,” in *IEEE International Parallel and Distributed Processing Symposium Workshops (IPDPSW)*, 2018, pp. 522–531.
- [7] N. P. Jouppi, C. Young, N. Patil *et al.*, “In-datacenter performance analysis of a tensor processing unit,” in *ACM/IEEE Annual International Symposium on Computer Architecture (ISCA)*, 2017, pp. 1–12.
- [8] D. Potts, G. Steidl, and M. Tasche, “Fast fourier transforms for nonequispaced data: A tutorial,” in *Modern Sampling Theory: Mathematics and Applications*, J. J. Benedetto and P. J. S. G. Ferreira, Eds. Boston, MA: Birkhäuser Boston, 2001, pp. 247–270.
- [9] S. Davis and P. Mermelstein, “Comparison of parametric representations for monosyllabic word recognition in continuously spoken sentences,” *IEEE Transactions on Acoustics, Speech, and Signal Processing*, vol. 28, no. 4, pp. 357–366, 1980.
- [10] M. Ravanelli and Y. Bengio, “Speaker recognition from raw waveform with SincNet,” in *IEEE Spoken Language Technology Workshop (SLT)*, 2018, pp. 1021–1028.
- [11] N. Zeghidour, O. Teboul, F. de Chaumont Quitry, and M. Tagliasacchi, “LEAF: A learnable frontend for audio classification,” in *International Conference on Learning Representations (ICLR)*, 2021.
- [12] J. Schlüter and G. Gutenbrunner, “EfficientLEAF: A faster LEArnable audio frontend of questionable use,” in *European Signal Processing Conference (EUSIPCO)*, 2022.

- [13] R. Sebastian, S. O’Keefe, and M. Trefzer, “Audio signal processing using time domain mel-frequency wavelet coefficient,” *arXiv preprint arXiv:2510.24519*, 2025. [Online]. Available: <https://arxiv.org/abs/2510.24519>
- [14] S. Bagchi and S. K. Mitra, *The Nonuniform Discrete Fourier Transform and Its Applications in Signal Processing*. Boston, MA: Springer, 1999.
- [15] A. J. W. Duijndam and M. A. Schonewille, “Nonuniform fast fourier transform,” *Geophysics*, vol. 64, no. 2, pp. 539–551, 1999.
- [16] J.-M. Lin, “Python Non-Uniform Fast Fourier Transform (PyNUFFT): An accelerated non-cartesian MRI package on a heterogeneous platform,” *Journal of Imaging*, vol. 4, no. 3, p. 51, 2018.
- [17] R. Schwartz, J. Dodge, N. A. Smith, and O. Etzioni, “Green AI,” *Communications of the ACM*, vol. 63, no. 12, pp. 54–63, 2020.
- [18] R. Caspart, S. Ziegler, A. Weyrauch *et al.*, “Precise energy consumption measurements of heterogeneous artificial intelligence workloads,” *arXiv preprint arXiv:2212.01698*, 2022.
- [19] B. McFee, C. Raffel, D. Liang *et al.*, “librosa: Audio and music signal analysis in Python,” in *Python in Science Conference (SciPy)*, 2015, pp. 18–25.
- [20] A. Nagrani, J. S. Chung, and A. Zisserman, “VoxCeleb: A large-scale speaker identification dataset,” in *Proceedings of Interspeech*, 2017, pp. 2616–2620.